Supplementary Information

Structural Modulation of Low-Cost Cu-Mn-Fe Prussian Blue Analogs for Long-Calendar-Life Sodium Ion Batteries

Yun Gao,[1,2,5] Hang Zhang,[3,5] Jinsong Wang,[4] Jian Peng,[3*] Yao Xiao,[1] Yang Liu,[1] Yun Qiao,[2] Li Li,[2*] Jiazhao Wang,[3] Shulei Chou[1*]

1. Institute for Carbon Neutralization, College of Chemistry and Materials Engineering, Wenzhou University, Wenzhou, Zhejiang 325035, China
2. School of Environmental and Chemical Engineering, Shanghai University, Shanghai, 200444, China
3. Institute for Superconducting and Electronic Materials, Australian Institute for Innovative Materials, University of Wollongong, Innovation Campus, Squires Way, North Wollongong, NSW 2522, Australia
4. Faculty of Materials Science and Engineering, Kunming University of Science and Technology, 650093 Kunming, P. R. China
5. These authors contributed equally.
*Correspondence to: jianp@uow.edu.au (J.Peng); lili2020@shu.edu.cn (L. Li); chou@wzu.edu.cn (S. Chou)

Method Section

Preparation of $Na_2Cu_{1-x}Mn_xFe(CN)_6$ samples, x = 0, 0.25, 0.5, 0.75, 1**.** All chemicals for the synthesis of PBAs were purchased from Aladdin and used directly without further purification. Typically, 10(1-n) mmol $MnSO_4•H_2O$, 10n mmol $CuSO_4•5H_2O$ and 20 mmol sodium citrate were mixed in 100 ml of deionized (DI) water to form solution A, and 20 mmol $Na_4Fe(CN)_6$ was put into 100 mmol DI water to obtain solution B after vigorous agitation. Solution A was slowly dropped into solution B by applying a peristaltic pump at the speed of 20 ml h^{-1} under continuous stirring, and then the combined solution was aged for 24 h at room temperature. The products were washed three times with DI water and once with ethanol to remove the impurities and unreacted raw materials. The final products were dried at 120 °C in a vacuum oven for 12 h. The obtained products were denoted as CuHCF-1, CuHCF-2, CuHCF-3, CuHCF-4, and MnHCF for x = 1, 0.75, 0.5, 0.25, and 0, respectively.

Materials characterization. The crystal structure of the samples was detected by powder X-ray diffraction (XRD, 18 kW D/MAX2500V+/PC, Smartlab, Rigaku Company) with a Cu Kα source. The XRD data was indexed and then refined by the Rietveld method with GSAS software. The thermogravimetry (TG) tests were carried out on a Netzsch TG209F3 analyzer in N_2 from 30 to 500 °C. The structures of samples were examined by Fourier transform infrared spectroscopy (FTIR, Nicolet 380 FTIR spectrometer, 4000-400 cm^{-1} region) and Raman spectroscopy (Renishaw in plus, excitation wavelength: 532 nm). A field emission scanning electron microscope (FESEM) with an energy dispersive X-ray spectrometer (EDS) and a high-resolution transmission electron microscope (HRTEM, JEM-2100F) were used to characterize the morphology, element composition and structure of all samples. The contents of Mn, Cu, and Fe were determined by inductively coupled plasma – optical emission spectroscopy (ICP-OES; IRIS Intrepid IIXSP, Thermo Elemental, USA). The surface information was collected by X-ray photoelectron

spectroscopy (XPS) with an Al Kα source (PHI ESCA-5000C). The *in-situ* laboratory XRD measurements were carried out on a Bruker D8 Advanced instrument (reflection mode, beryllium windows), using thinner Al foil as the current collector, and the interval term was set at 720 s for each 2θ scan.

Electrochemical measurements. The cathode electrode slurry for 2032-coin cell testing was prepared by mixing 70 wt% active materials (PBA), 20 wt% Ketjen black (KB), and 10 wt% carboxymethyl cellulose (CMC) in water. The slurry was coated evenly on the Al foil and then dried at 100 °C for 12 h in a vacuum oven. Sodium metal, glass fiber (Whatman, GF/D), and 1 M $NaClO_4$ in ethylene carbonate and diethyl carbonate (v/v = 1:1) with 5 % fluoroethylene carbonate additive served as the counter electrode, the separator, and the electrolyte, respectively. The cells were assembled in an argon-filled glove box with H_2O and O_2 concentrations less than 0.01 ppm. The electrochemical properties, including cycling, rate performance and so on, were tested by applying a Neware battery cycler (CT-4008-5V10mA-164, Shenzhen, China) with a potential range from 2.0 to4.2 V. Cyclic voltammetry (CV) under different scan rates was conducted on a CHI760D electrochemical workstation from 2.0 to 4.2 V. The full cell was assembled using hard carbon (HC) without any activation and CuHCF-3 as anode and cathode, respectively. Notably, the HC anode electrodes were prepared by the same procedures as the cathode electrodes, except that the slurry was prepared by mixing 95 wt% active materials (HC) and 5 wt% sodium alginates (SA) in water. The specific capacity of the full cell was calculated based on the mass of cathode materials, and charge/discharge tests were conducted over the voltage range of 1.7-3.8 V. Activation was performed in high-/low-temperature tests. The cathode was fully charged and discharged at 10 mA g^{-1} within the potential range of 2.0-4.2 V at room temperature to form a dense and stable cathode-electrolyte interphase (CEI).

Supplementary Figures

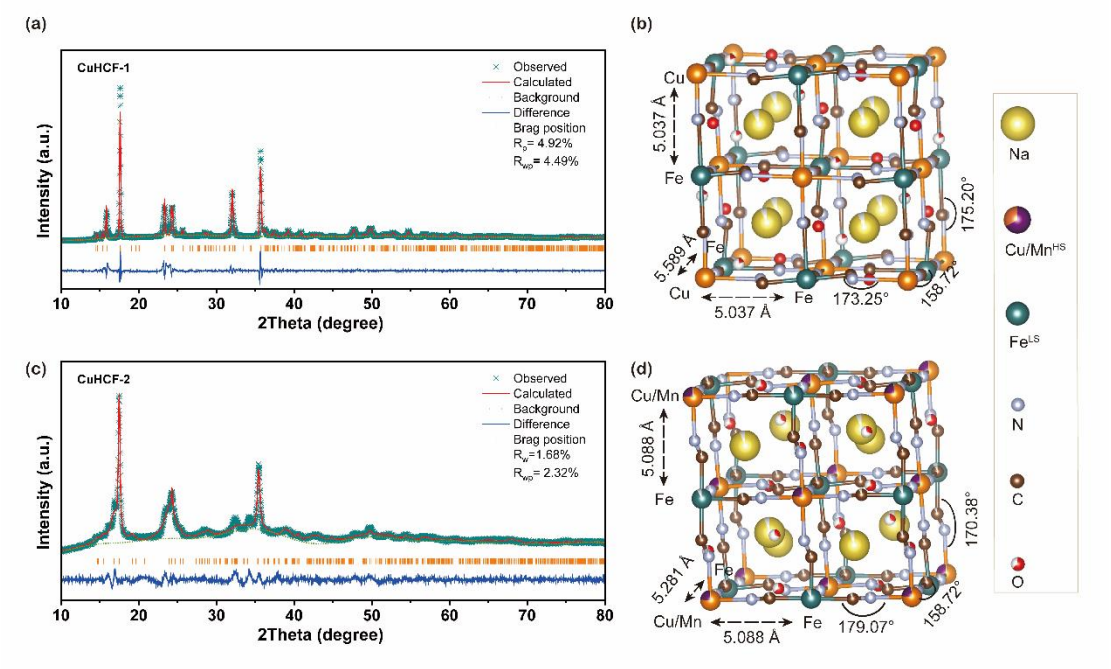

Figure S1. Rietveld refinements and local structures of the (a, b) monoclinic CuHCF-1 and (c, d) monoclinic phase CuHCF-2.

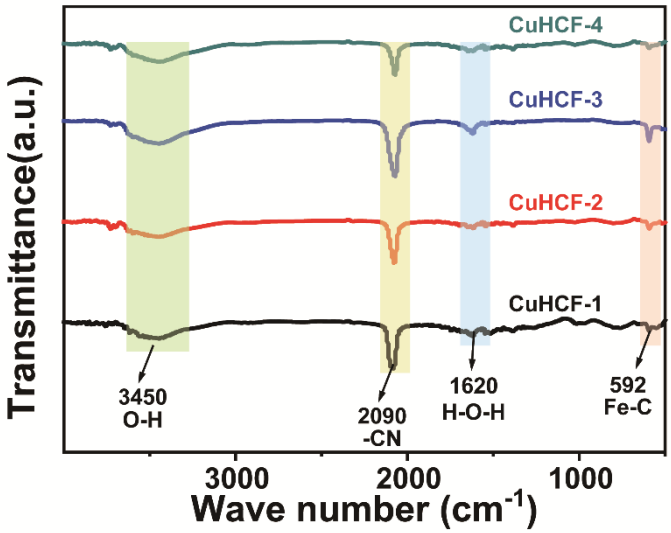

Figure S2. FTIR spectra of the four as-prepared samples.

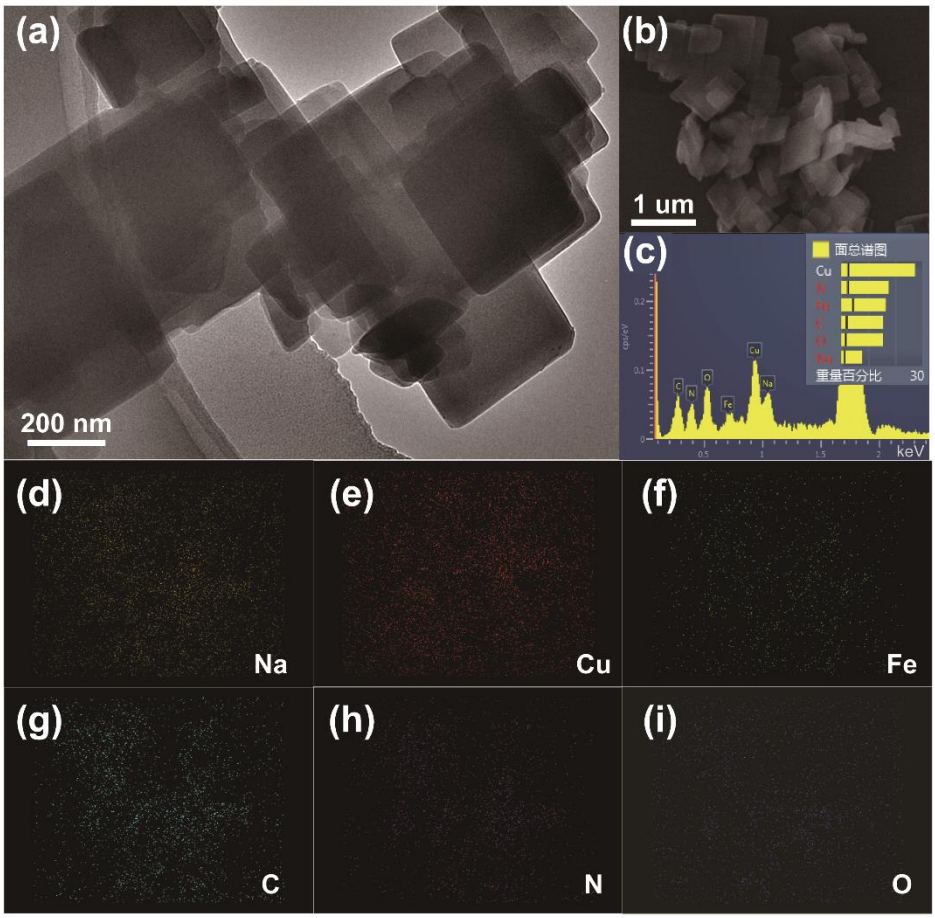

Figure S3. (a) Transmission electron microscope (TEM) image, (b) scanning electron microscope (SEM) image, (c) energy dispersive spectroscopy (EDS) analysis, and (d-i) mapping images of Na, Cu, Fe, C, N, and O elements of the as-prepared CuHCF-1.

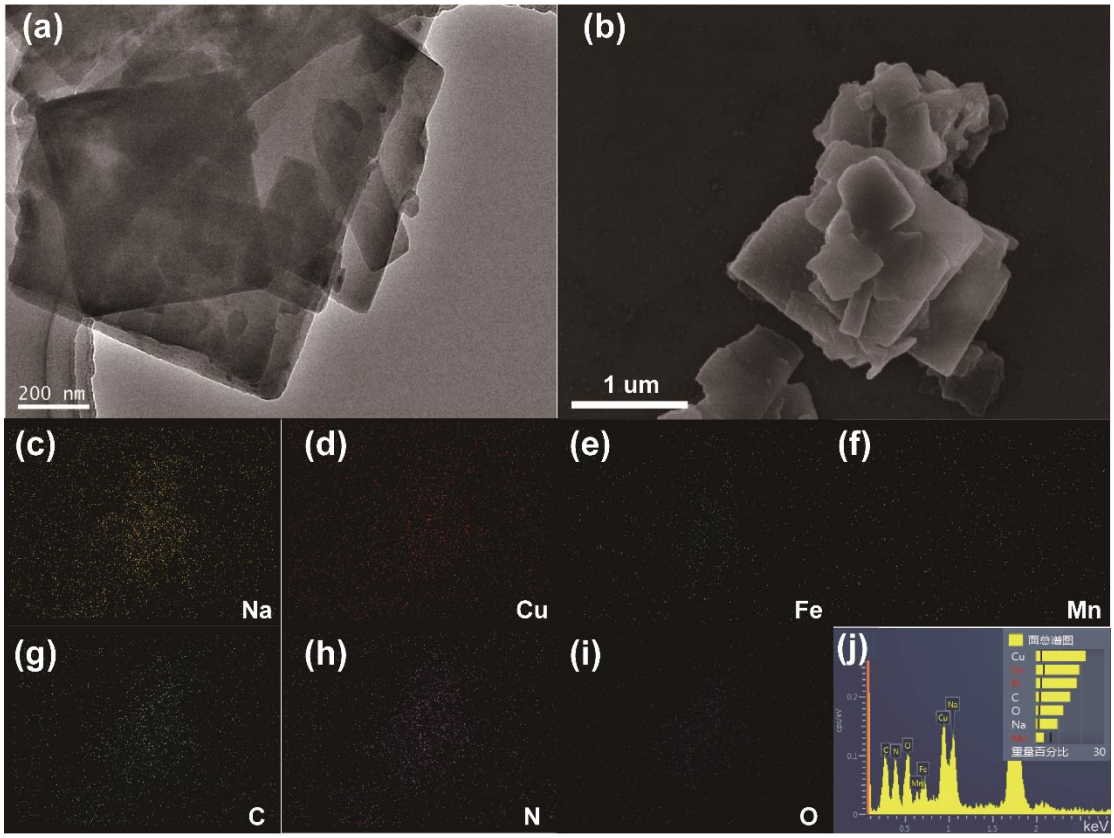

Figure S4. (a) TEM image, (b) SEM image, (c-i) mapping images of Na, Cu, Fe, Mn, C, N, and O elements, and (j) EDS analysis of the as-prepared CuHCF-2.

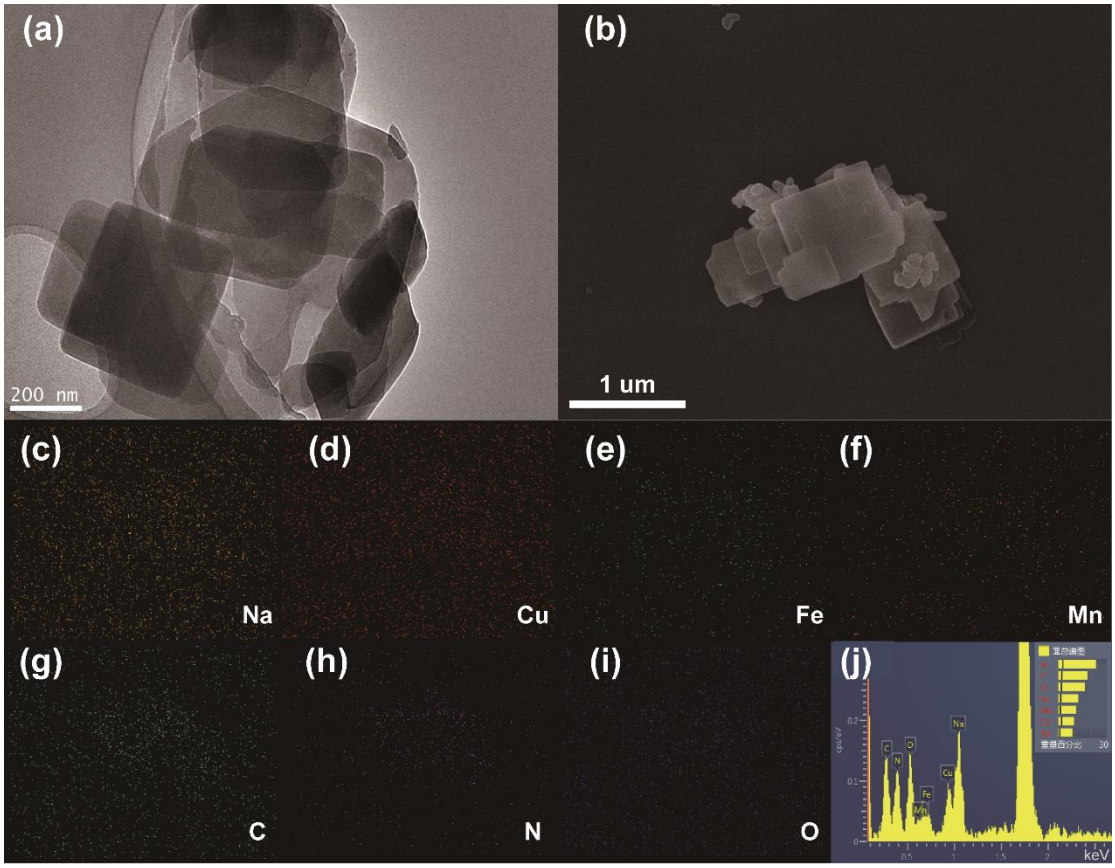

Figure S5. (a) TEM image, (b) SEM image, (c-i) mapping images of Na, Cu, Fe, Mn, C, N, and O elements, and (j) EDS analysis of the as-prepared CuHCF-4.

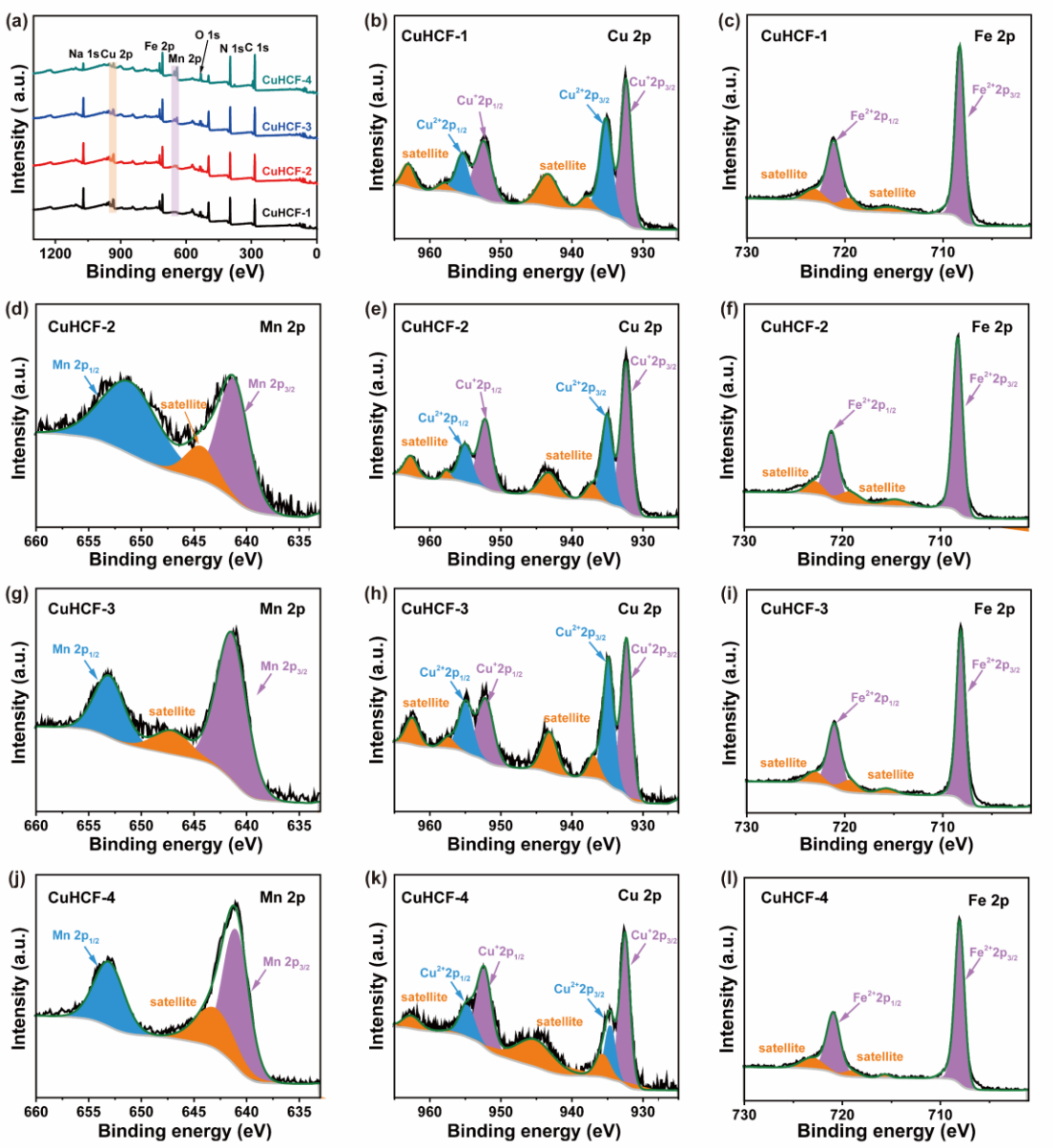

Figure S6. X-ray photoelectron spectroscopy (XPS) analysis of the four samples. (a) Survey spectra, (d, g, j) Mn 2p XPS spectra of CuHCF-2, CuHCF-3, and CuHCF-4, respectively. (b, e, h, k) Cu 2p XPS spectra and (c, f, i, l) Fe 2p spectra of CuHCF-1, CuHCF-2, CuHCF-3, and CuHCF-4, respectively.

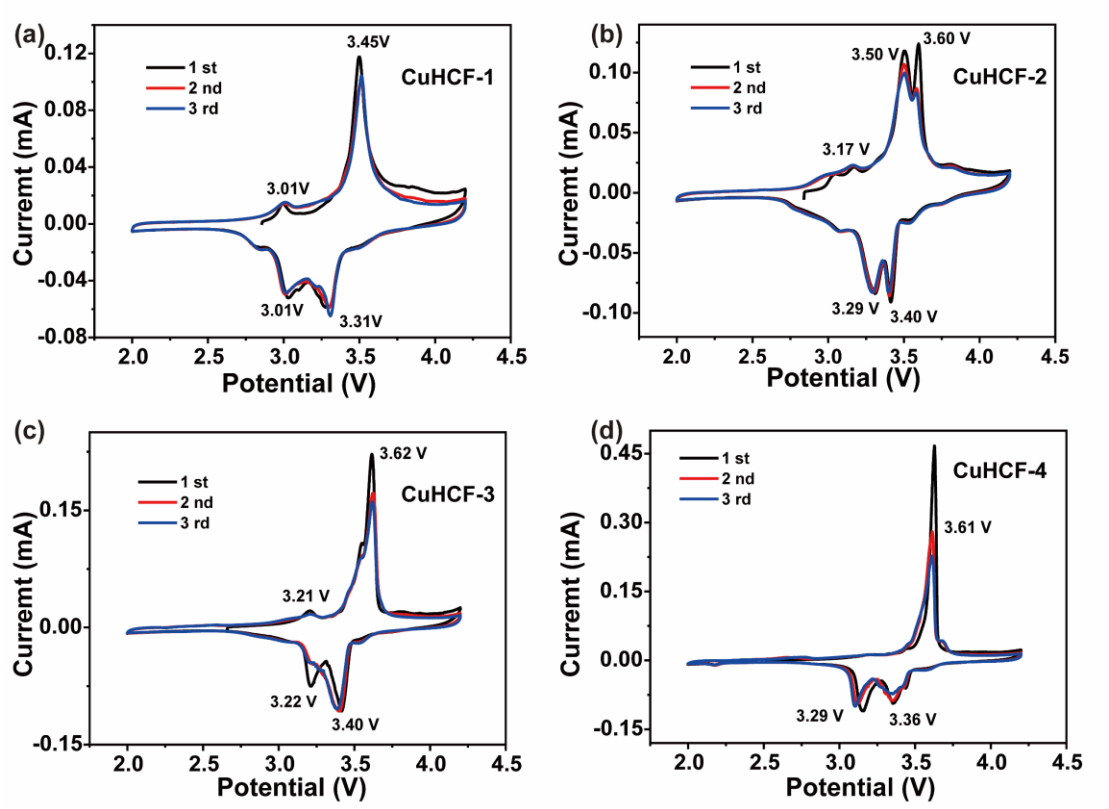

Figure S7. CV curves of the first three cycles for (a) CuHCF-1, (b) CuHCF-2, (c) CuHCF-3, and (d) CuHCF-4.

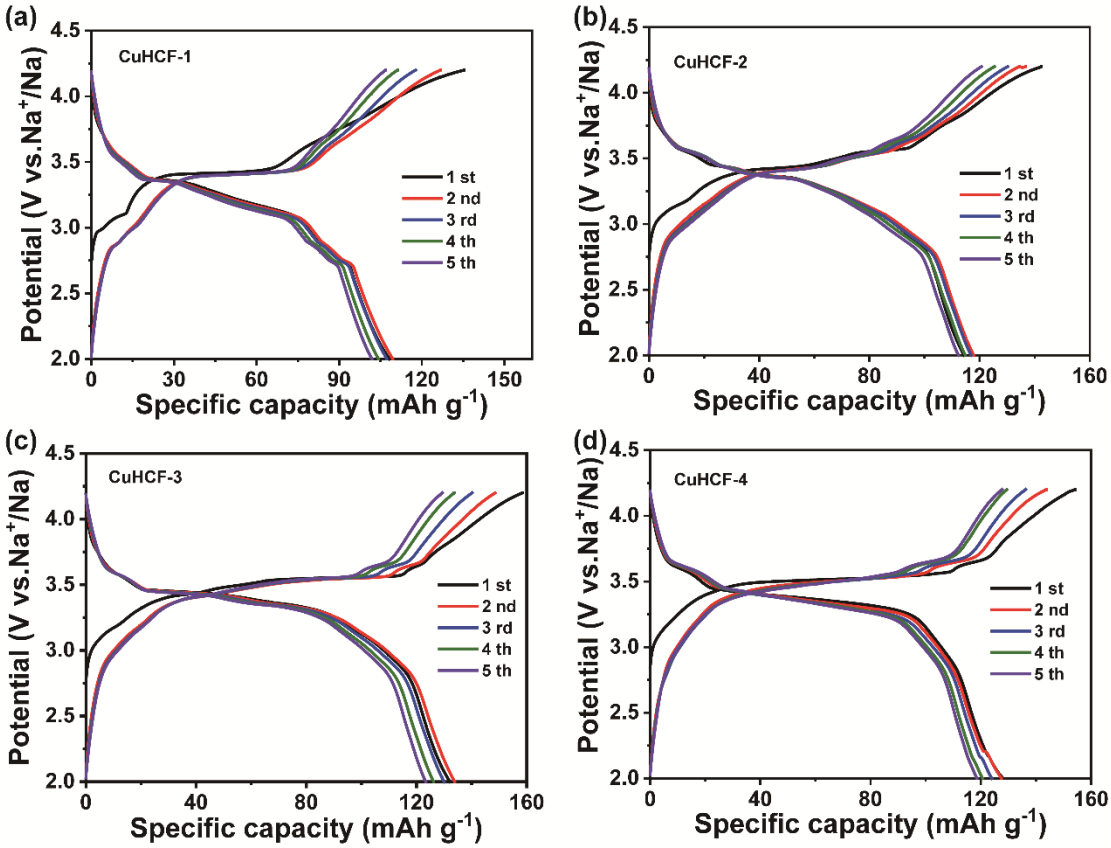

Figure S8. Galvanostatic charge-discharge (GCD) profiles of the first five cycles for the four samples.

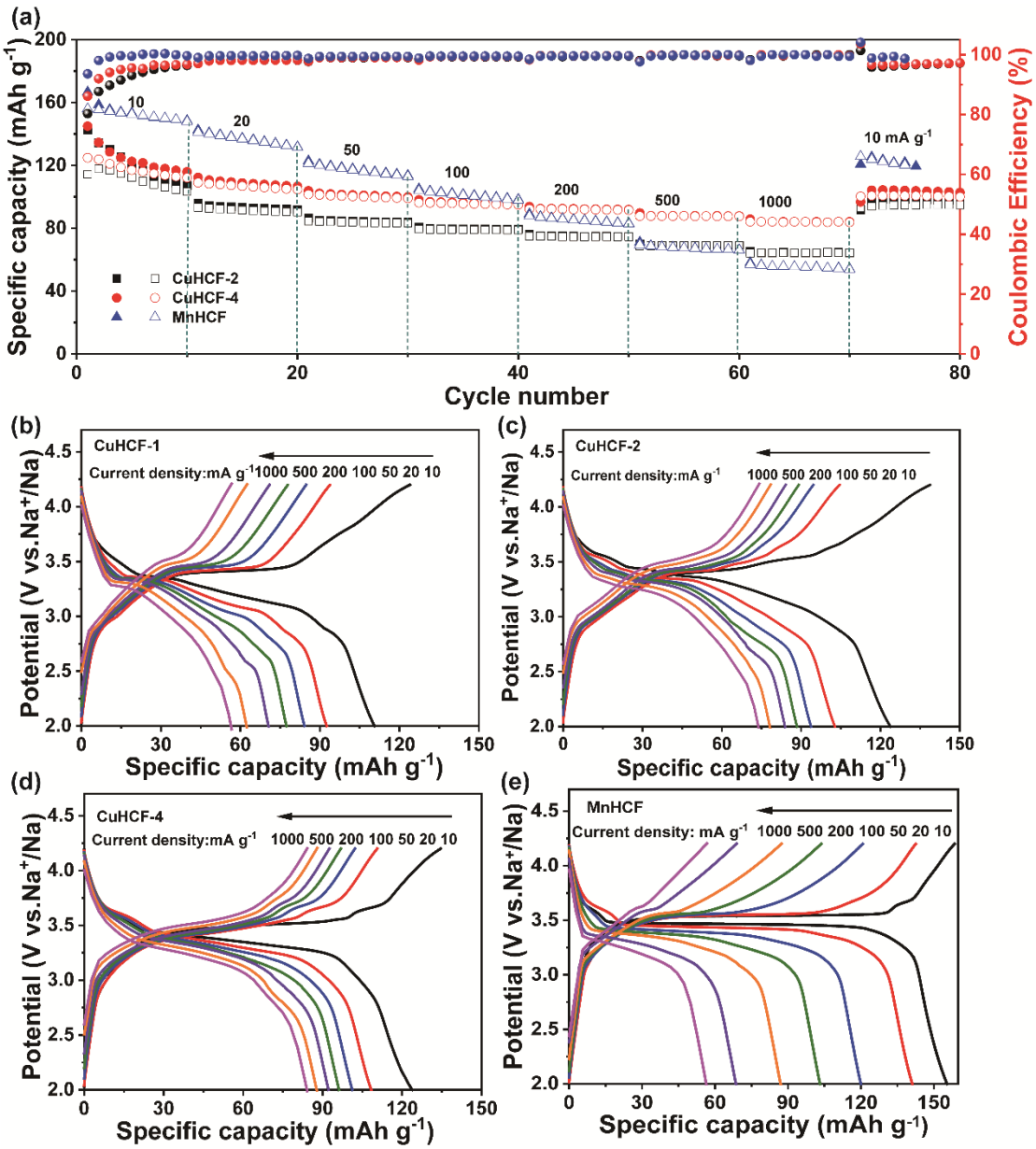

Figure S9. (a) Rate performances of CuHCF-2, CuHCF-4, and MnHCF at various current densities from 10 to 1000 mA g^{-1}. GCD curves over a current density range of 10-1000 mA g^{-1} for (b) CuHCF-1, (c) CuHCF-2, (d) CuHCF-4, and (e) MnHCF.

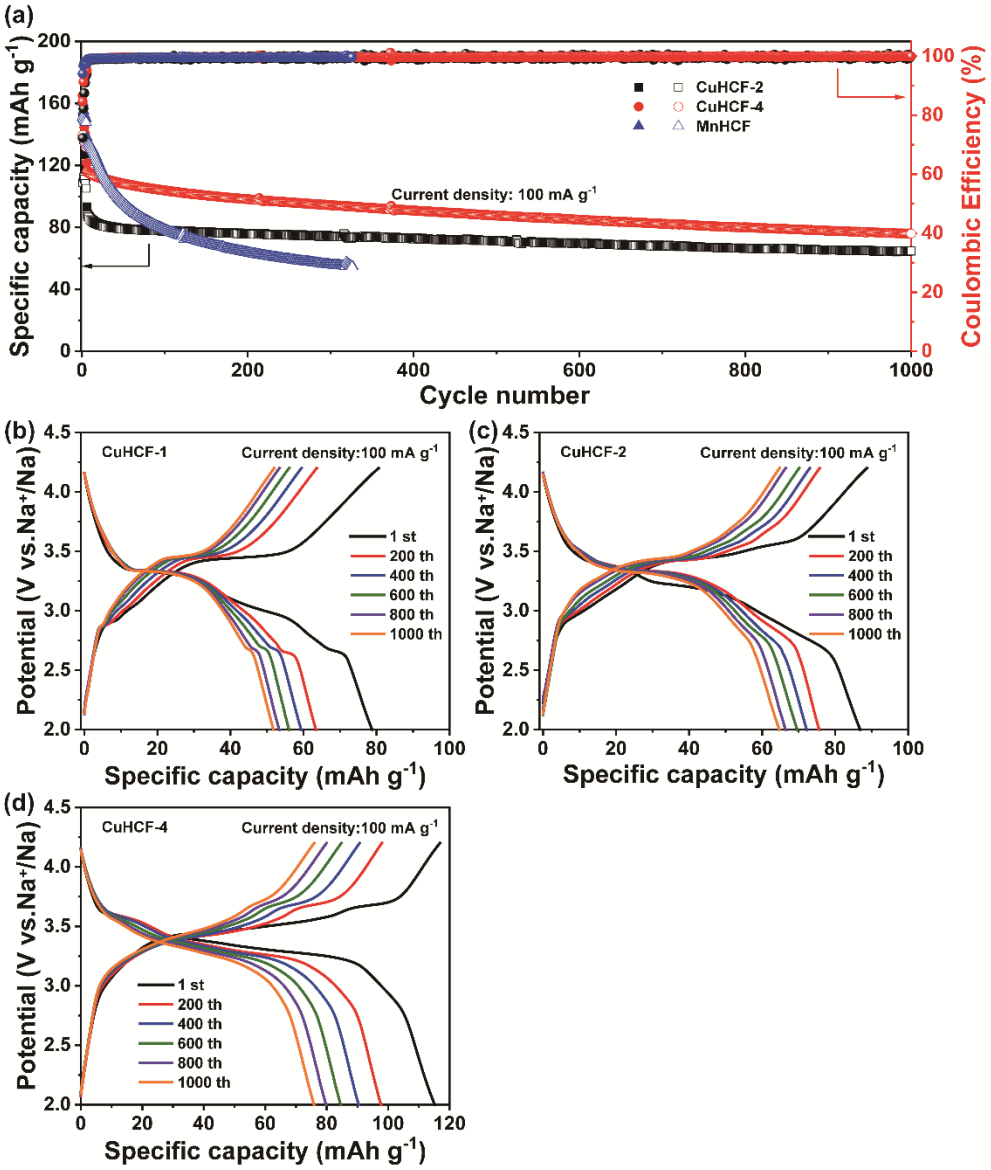

Figure S10. (a) Cycling performances of CuHCF-1, CuHCF-2, and CuHCF-4 at a current density of 100 mA g^{-1}. GCD curves at 100 mA g^{-1} for (b) CuHCF-1, (c) CuHCF-2, and (d) CuHCF-4.

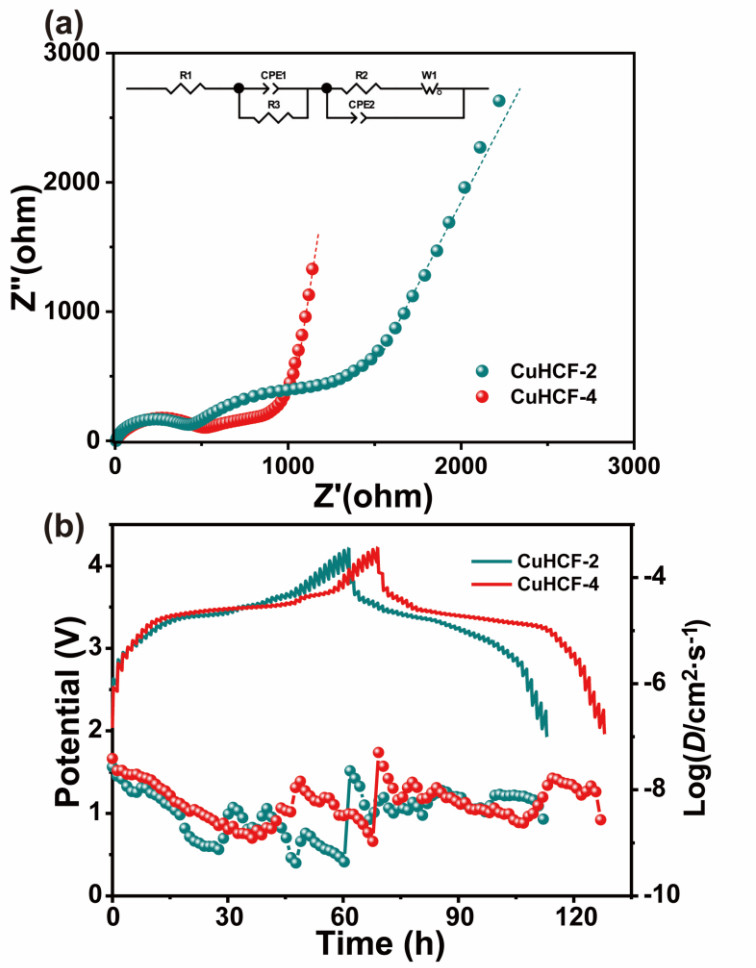

Figure S11. (a) Electrochemical impedance spectra (EIS) over the frequency range of 0.01-100 kHz, (b) GITT profiles and corresponding calculations for CuHCF-2 and CuHCF-4.

The D_{Na+} was calculated according to the equation (1): [1,2]

$$D_{Na^+} = \frac{4}{\pi\tau}\left(\frac{m_B V_m}{M_B S}\right)^2 \left(\frac{\Delta E_S}{\Delta E_\tau}\right)^2 \left(\tau \ll \frac{L^2}{D_{Na^+}}\right), \quad (1)$$

Where m_B, V_m, and M_B represent the active mass, the molar volume, and the molar mass of all samples, respectively. τ, S, ΔE_s, and ΔE_τ represent the duration of a current pulse, the effective surface of the cathode, the potential gap between the two steady-state plateaus in a single-step GITT process, and the voltage variation during a current pulse.

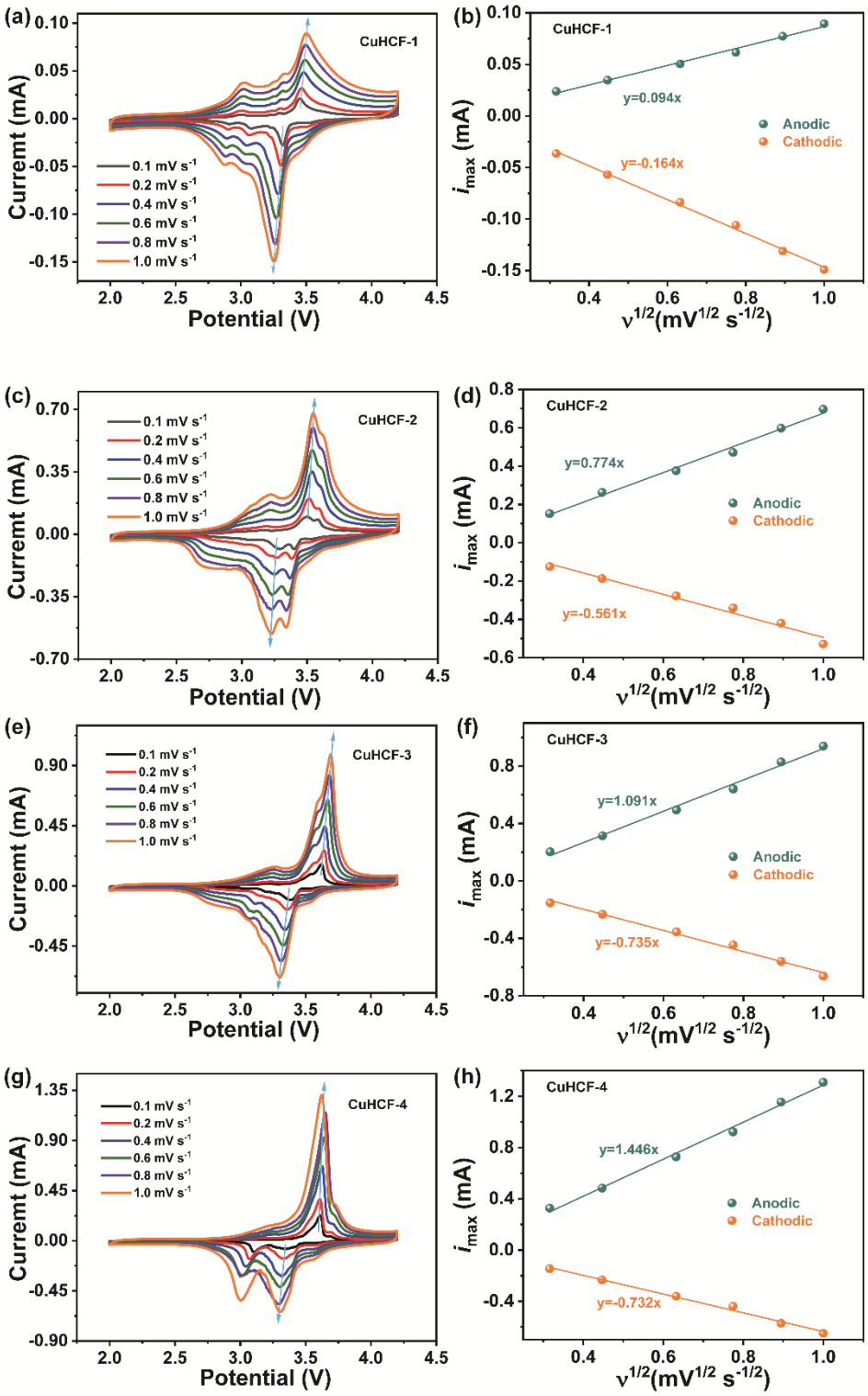

Figure S12. CV curves at various scanning rates (left) and peak current at each scan rate plotted versus the square root of the scanning rate (right): (a, b) CuHCF-1, (c, d) CuHCF-2, (e, f) CuHCF-3, and (g, h) CuHCF-4.

CV tests at various sweep rates were performed to evaluate the D_{Na+} of the

CuHCF-t (t = 1, 2, 3, and 4) electrodes. According to the slope of the peak current versus the square root of the scan rate ($v^{1/2}$), the D_{Na+} was calculated based on the following Randles-Sevcik Equation (2):[1,3,4]

$$I_p = 0.4463\, n^{3/2} F^{3/2} C S R^{-1/2} T^{-1/2} D_{cv}^{1/2} v^{1/2} \quad (2)$$

where I_p (A), n, F, C (mol cm^{-3}), S (cm^2), R, T (K), $D_{Na+,}$ and v (V s^{-1}) represent the peak current, the number of electrons transferred during a redox reaction, the Faraday constant (96485 C mol^{-1}), the Na-ion concentration in moles in the single unit cell (mol cm^{-3}), the effective area of the positive electrode, the gas constant (8.314 J mol^{-1} K^{-1}), the absolute temperature, the Na^+ diffusion coefficient, and the potential scan rate in volts per second, respectively.

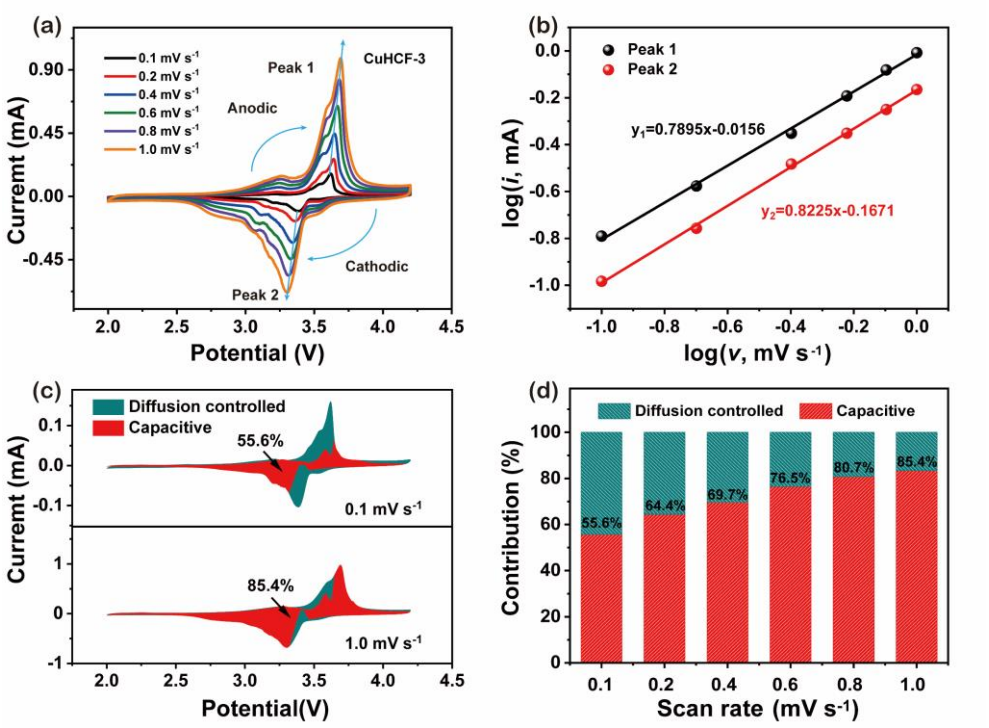

Figure S13. **Electrochemical kinetics analyses of sodium storage for CuHCF-3.** (a) Normalized CV curves at various scan rates. (b) Determination of slope values from the linear fitting. (c) Capacitive contribution at scan rates of 0.1 and 1.0 mV s^{-1}. (e) Contribution ratio of capacitive current to diffusion-controlled current versus scan rate.

The capacitive contribution was further analyzed according to the following Equations (3) and (4): [5,6]

$$i(V) = k_1 v + k_2 v^{1/2} \quad (3)$$

where $k_1 v$ is ascribed to the capacitive-controlled process and $k_2 v^{1/2}$ to the diffusion-controlled reactions.

Equation (3) was rearranged for easy analytical purposes as the following Equation (4):

$$I(V)/ v^{1/2} = k_1 v^{1/2} + k_2 \quad (4)$$

where i is the peak current (mA), v represents the various scan rates, and k_1 and k_2 are constants.

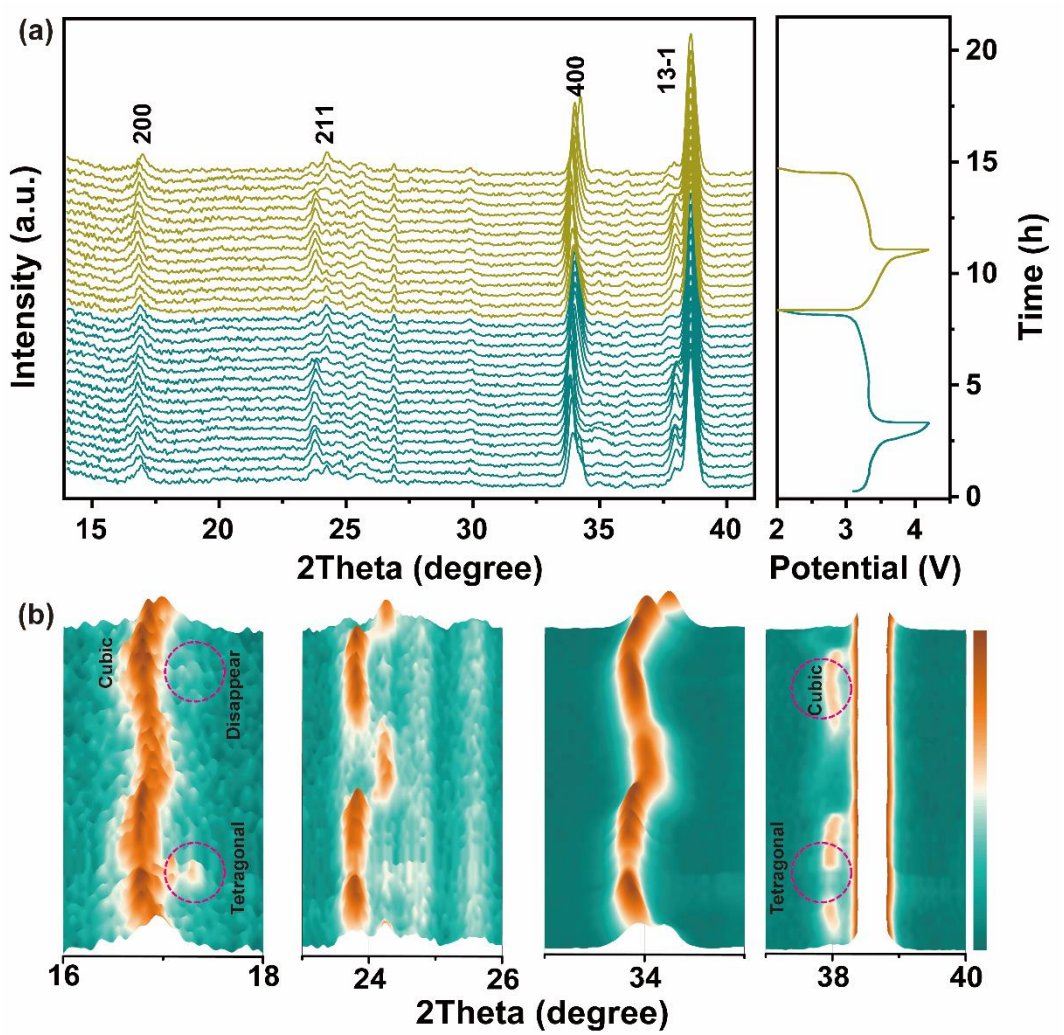

Figure S14. *In-situ* XRD analysis of the MnHCF. (a) *In-situ* XRD patterns (left) with the corresponding GCD profile at 30 $mA \cdot g^{-1}$ (right) of the (200), (211), (400), and (13-1) reflection planes, with the 2D corresponding contour plots in (b) from left to right, respectively, for the MnHCF.

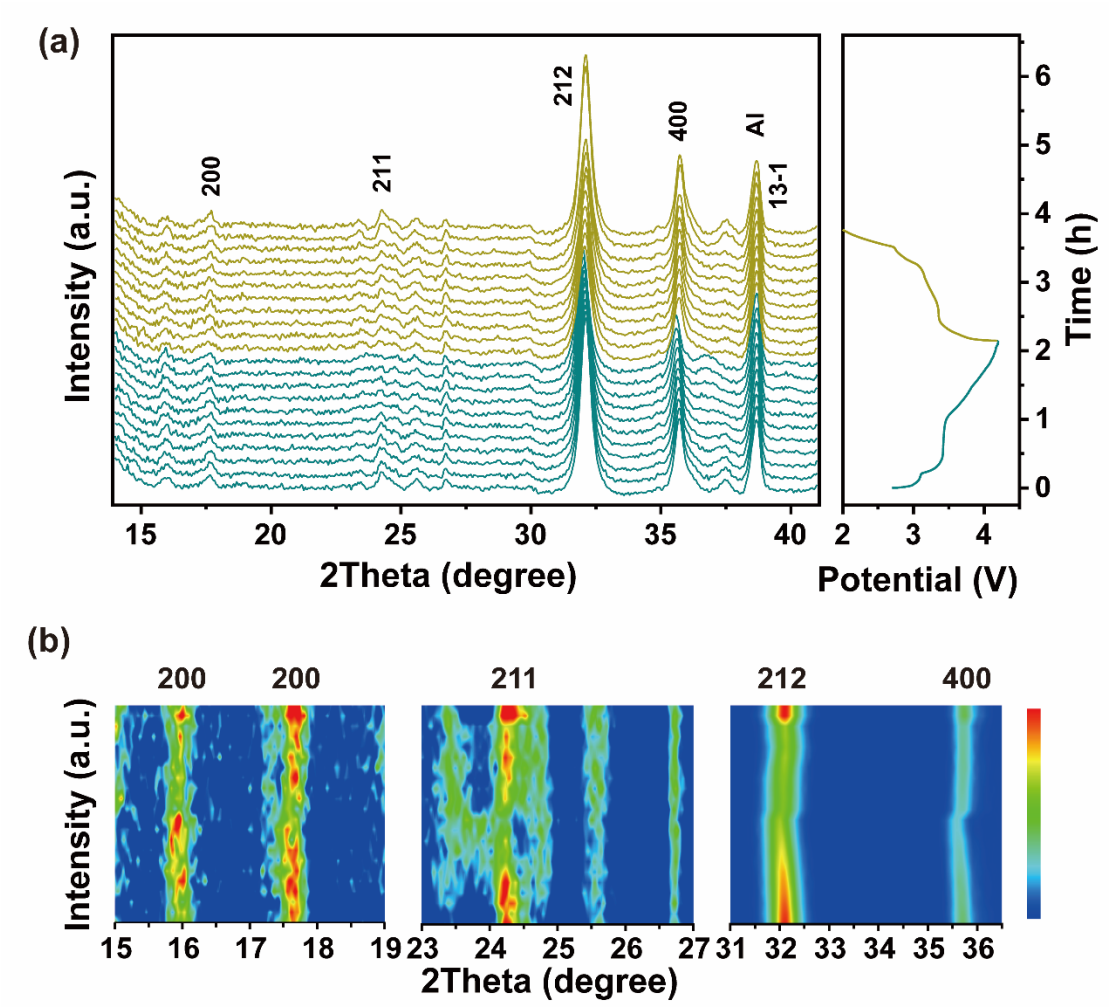

Figure S15. In situ XRD analysis of the CuHCF-1. (a) In situ XRD patterns of the (200), (211), (212), (400), and (13-1) reflection planes (left), and the corresponding GCD profile at 30 mA g^{-1} (right). (b) 2D contour plots of the (011), (211), (212), and (400) planes for the CuHCF-1.

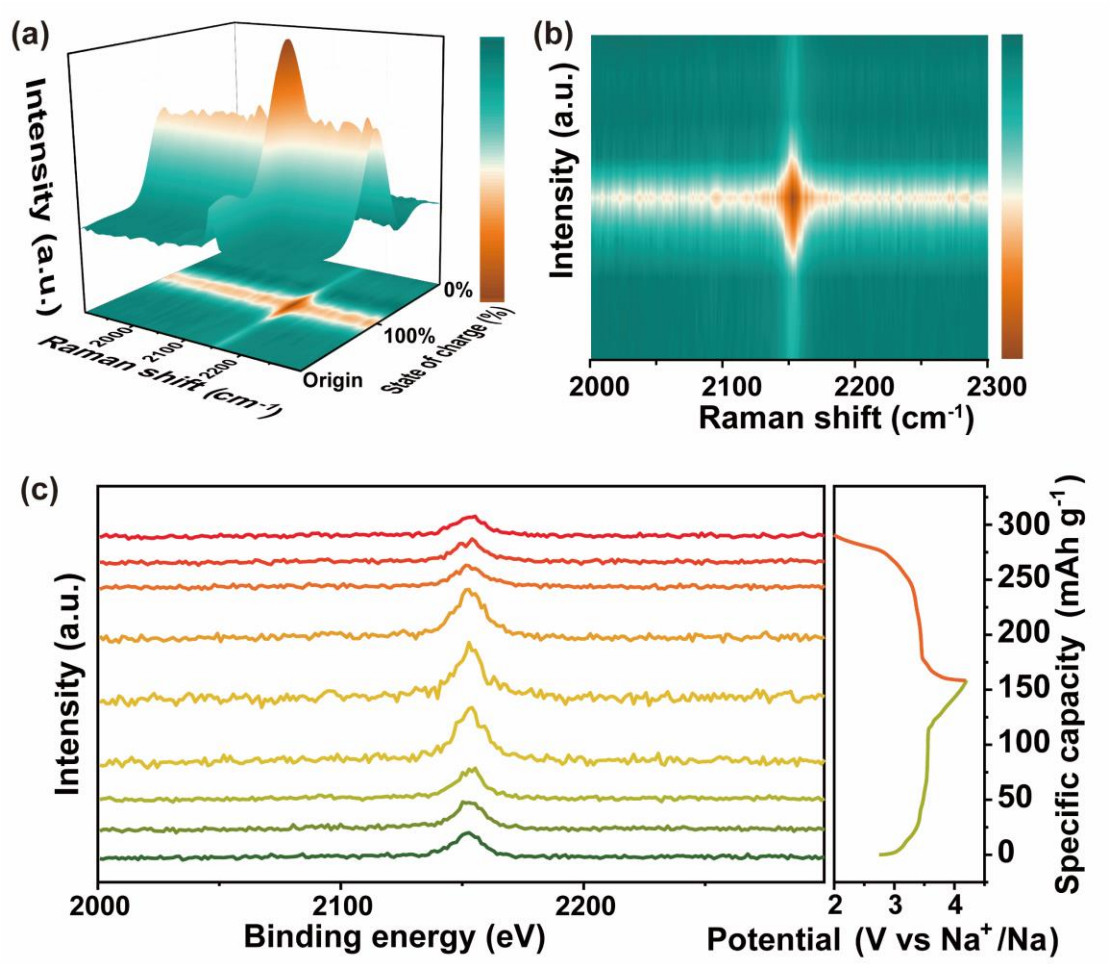

Figure S16. *In-situ* Na-ion storage mechanism analysis by Raman measurements of CuHCF-3: (a) 3D colormap surface with projection, (b) 2D contour graph, and (c) Raman spectra during charge-discharge (left) and corresponding GCD profile at 30 mA g^{-1} (right).

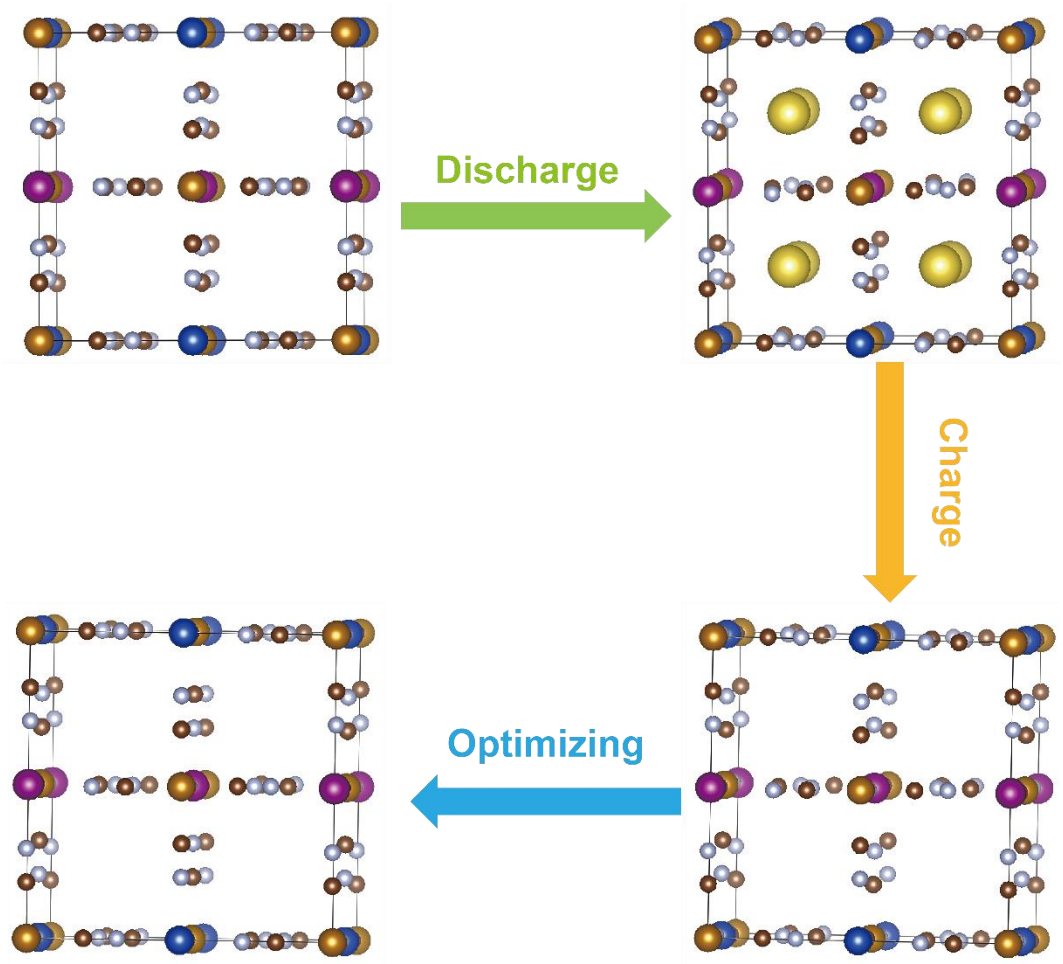

Figure S17. The structural stability of CuHCF-3 based on DFT calculations.

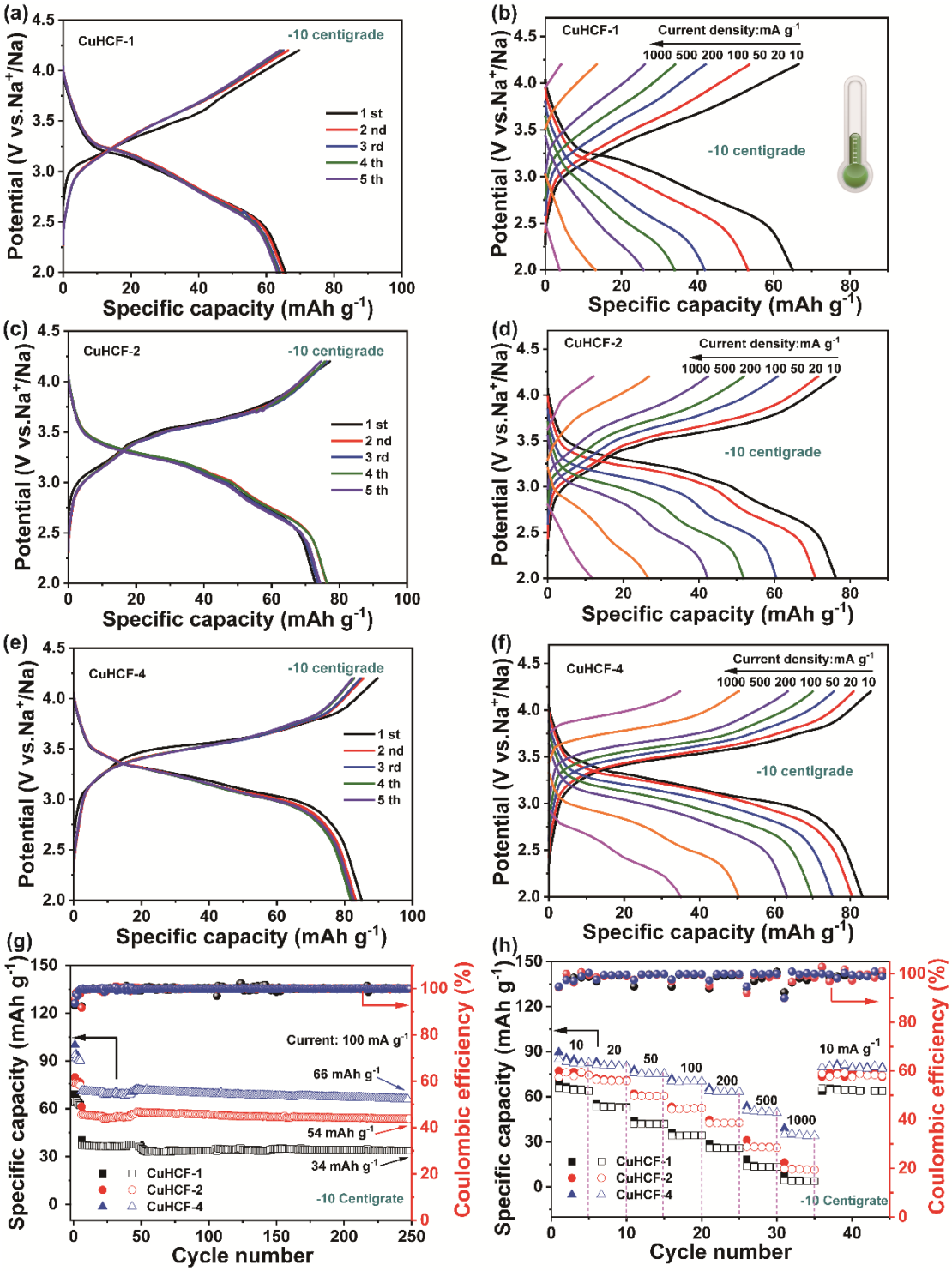

Figure S18. The electrochemical performances at -10 °C for CuHCF-1, CuHCF-2, and CuHCF-4. (a, c, e) The first five GCD curves under a current density of 10 mA g^{-1}. (b, d, f, h) Rate performances at various current densities from 10 to 1000 mA g^{-1}. (g) Long-term cycling performances with a current density of 100 mA g^{-1}.

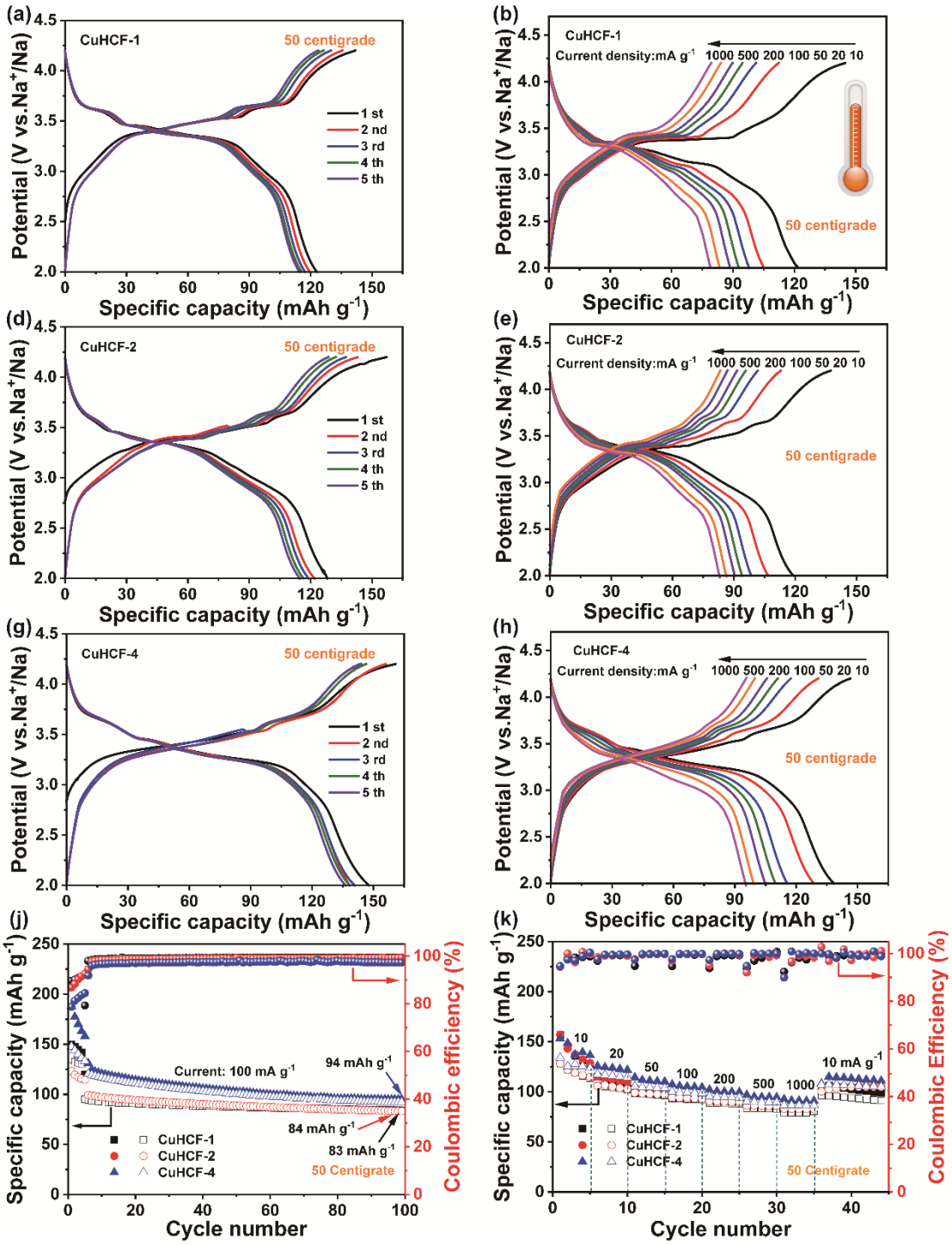

Figure S19. The electrochemical properties at 50 °C of CuHCF-1, CuHCF-2, and CuHCF-4. (a, c, e) The initial five GCD curves at 10 mA g^{-1}. (b, d, f, h) Rate performances at different current densities from 10 to 1000 mA g^{-1}. (g) Long-term cycling performances at a current density of 100 mA g^{-1}.

Supplementary Tables

Table S1 Detailed structural information on the CuHCF-1 sample after Rietveld refinement based on XRD data.

CuHCF-1: Monoclinic, space group P21/n, *a*=11.1783 Å, *b*=7.2939 Å, *c*=6.9499 Å, *α*=90.0000°, *β*= 92.9270°, *γ*=90.0000°, *V*=565.907608 Å^3. *U*: isotropic thermal parameter (Å^2).						
Atom	x	y	z	Occupation	U	Site
N1	0.46271	0.22692	0.75872	0.998	0.242	4e
N2	0.25899	0.49513	0.49976	0.998	0.024	4e
N3	0.49355	0.28343	0.26719	0.998	0.013	4e
C1	0.52826	0.19357	0.76648	0.998	0.209	4e
C2	0.17931	0.49106	0.50191	0.998	0.021	4e
C3	0.48259	0.27587	0.272	0.998	0.038	4e
Na	0.23903	0.47989	0.01513	0.926	0.027	4e
Cu	0.50000	0.50000	0.50000	1.000	0.029	2a
O1	0.2588	0.42195	0.66932	0.184	0.107	4e
O2	0.24183	0.21183	0.25637	1.000	0.003	4e
Fe	0.50000	0.00000	1.00000	0.998	0.001	2d

Table S2 Detailed structural information on the CuHCF-2 sample after Rietveld refinement based on XRD data.

CuHCF-2: Monoclinic, space group P21/n, *a*=10.56300 Å, *b*=7.34810 Å, *c*=7.03910 Å, *α*=*γ*=90.0000°, *β*=87.5600°, *V*=545.865380 Å^3						
Atom	x	y	z	Occupation	U	Site
N1	0.00366	0.20331	0.20650	0.91400	0.08500	4e
N2	0.30075	0.51215	0.50141	0.91400	0.10700	4e
N3	0.00043	0.79514	0.22565	0.91400	0.18600	4e
C1	0.02615	0.29070	0.30734	0.91400	0.02100	4e
C2	0.18080	0.50940	0.55634	0.91400	0.08700	4e
C3	0.03644	0.68710	0.28811	0.91400	0.17400	4e
Fe	0.00000	0.50000	0.50000	0.91400	0.01400	2d
Cu	0.00000	0.00000	0.00000	0.76000	0.09000	2a
Na	0.16263	0.53109	0.05325	0.93600	0.05400	4e
O	0.22312	0.48933	0.07880	0.30100	0.06900	4e
O2	0.09462	0.23949	0.77618	0.64000	0.00200	4e
Mn	0.00000	0.00000	0.00000	0.23100	0.07800	2a

Table S3 Detailed structural information on the CuHCF-3 sample after Rietveld refinement based on XRD data.

CuHCF-3: Monoclinic, space group P21/n, *a*=10.4596 Å, *b*=7.5462 Å, *c*=6.9204 Å, *α*=*γ*=90.0000°, *β*=88.86300°, *V*=546.121259 Å^3						
Atom	x	y	z	Occupation	U	Site
N1	0.00548	0.19376	0.23122	1.00000	0.56100	4e
N2	0.28928	0.52667	0.52361	1.00000	0.01000	4e
N3	0.01038	0.83920	0.20192	1.00000	0.01300	4e
C1	0.00822	0.28941	0.32080	1.00000	0.00700	4e
C2	0.20469	0.52985	0.39006	1.00000	0.08300	4e
C3	0.00049	0.67808	0.29424	1.00000	0.05500	4e
Fe	0.00000	0.50000	0.50000	1.00000	0.12200	2d
Mn	0.00000	0.00000	0.00000	0.40400	0.14200	2a
Na	0.22261	0.54614	0.02532	1.00000	0.02900	4e
O	0.09571	0.44517	0.17856	0.59400	0.18500	4e
O2	0.22004	0.13631	0.79829	0.63500	0.02300	4e
Cu	0.00000	0.00000	0.00000	0.59600	0.03800	2a

Table S4 Detailed structural information on the CuHCF-4 sample after Rietveld refinement based on XRD data.

CuHCF-2: Cubic, space group Fm-3m, $a=b=c$=10.40760 Å, $\alpha=\beta=\gamma$=90.0000°, V=1127.331981 Å^3						
Atom	x	y	z	Occupation	U	Site
Na	0.25000	0.25000	0.25000	1.00000	0.06000	8c
Fe	0.00000	0.00000	0.00000	0.99300	0.02600	4a
Mn	0.00000	0.00000	0.50000	0.66900	0.07400	4b
C	0.00000	0.00000	0.19635	0.99300	0.03800	24e
N	0.00000	0.00000	0.24694	0.99300	0.04500	24e
Cu	0.00000	0.00000	0.50000	0.33100	0.02800	4b

Table S5 ICP-OES results on Mn, Fe, Cu for CuHCF-1, CuHCF-2, CuHCF-3, and CuHCF-4 samples.

Sample	Element content (wt%)				Chemical composition
	Na	Cu	Mn	Fe	
CuHCF-1	7.4845	13.3306	-	8.3536	$Na_{1.55}Cu[Fe(CN)_6]_{0.71}\cdot 2.80H_2O$
CuHCF-2	6.6210	7.1096	3.3293	8.2312	$Na_{1.67}Cu_{0.65}Mn_{0.35}[Fe(CN)_6]_{0.85}\cdot 3.22H_2O$
CuHCF-3	9.9003	6.1314	7.4169	10.8961	$Na_{1.86}Cu_{0.42}Mn_{0.58}[Fe(CN)_6]_{1.00}\cdot 2.26H_2O$
CuHCF-4	8.8462	6.8317	10.9413	10.9437	$Na_{1.42}Cu_{0.26}Mn_{0.74}[Fe(CN)_6]_{0.72}\cdot 2.49H_2O$

References

[1] F. Gebert, D. L. Cortie, J. C. Bouwer, W. Wang, Z. Yan, S.-X. Dou, S.-L. Chou, *Angew. Chem.* **2021**, *133*, 18667.

[2] Z.-Y. Chen, X.-Y. Fu, L.-L. Zhang, B. Yan, X.-L. Yang, *ACS Applied Materials & Interfaces* **2022**, *14*, 5506.

[3] S. Wheeler, I. Capone, S. Day, C. Tang, M. Pasta, *Chem. Mater.* **2019**, *31*, 2619.

[4] X. Pu, H. Wang, T. Yuan, S. Cao, S. Liu, L. Xu, H. Yang, X. Ai, Z. Chen, Y. Cao, *Energy Storage Materials* **2019**, *22*, 330.

[5] W. Ren, Z. Zhu, M. Qin, S. Chen, X. Yao, Q. Li, X. Xu, Q. Wei, L. Mai, C. Zhao, *Adv. Funct. Mater.* **2019**, *29*, 1806405.

[6] Y. Mao, Y. Chen, J. Qin, C. Shi, E. Liu, N. Zhao, *Nano Energy* **2019**, *58*, 192.